Analytic Solution for Transcranial Direct Current Stimulation

Matthew Palermo

June 26, 2014

Abstract

An analytic, prolate spheroidal solution to a transcranial direct current stimulation model which uses accurate electrode boundary conditions has been developed. This solution is intended to be compared against other solutions to the model to check the accuracy of the solutions. The solution approximates the shape of the human head as a prolate spheroid and approximates the electrical conductivity of the head as constant in 'shells'.

The spheroidal solution was compared against a recently developed spherical solution. The spheroidal and spherical solution is shown to give the same results for most cases. For some cases the solutions do not yield the same results and some reasons why has been hypothesised.

Finally the use of the model as a clinical tool was demonstrated by using the spheroidal solution to investigate the electric field distribution within the human head during transcranial direct current stimulation treatments using different electrode placements.

1 Introduction

1.1 Transcranial Direct Current Stimulation (tDCs)

For the AMSI vacation research scholarship program, work was done towards developing a clinical tool for researching and using the *transcranial direct current stimulation* medical treatment. Transcranial direct current stimulation, abbreviated as tDCs, is a primitive medical treatment where electrodes are placed on the surface of a patient's scalp and are used to pass low amplitude direct current electricity through the patient's head in order to stimulate the brain. Interest in tDCs has increased in the past few decades and clinical trials have shown that tDCs can effectively treat mental illnesses such as Alzheimer's disease, Parkinson's disease and Dementia [1].

Unfortunately without a mathematical model of tDCs, the exact effect that a tDCs treatment will have on a patient is difficult to predict. So an accurate mathematical model of the treatment would be a very useful clinical tool in researching and using tDCs safely.

1.2 Modelling tDCs

1.2.1 The electromagnetic field

The treatment induces a change in the electromagnetic field and the electric current so a useful tDCs clinical tool/model would model the electromagnetic field and electric current inside the patient's head. It has been established that the physics of classical electromagnetism is a fairly accurate description at the human scale and since tDCs is often used with only constant (or very slowly varying) amplitude electric current, the electromagnetic field can be modelled by the time static Maxwell's equations. Additionally the electric current passed through the electrodes do not exceed 1mA so it can be assumed that the relation between the electric field and the electric current density within the human head is approximately linear. From now on, Let $\Omega \subset \mathbb{R}^3$ be a closed, connected subset of Euclidean space which represents the space inside of the patient's head and $\mathbf{x} \in \Omega$ be some point inside the patient's head. By using the time static Maxwell's equations and the approximation of linear current density, the electric field and current can be modelled by equations (1,2,3)

$$\nabla \cdot \sigma(\mathbf{x}) \nabla u(\mathbf{x}) = 0 \tag{1}$$

$$\mathbf{E}(\mathbf{x}) = -\nabla u(\mathbf{x}) \tag{2}$$

$$\mathbf{J}(\mathbf{x}) = \sigma(\mathbf{x})\mathbf{E}(\mathbf{x}) = -\sigma(\mathbf{x})\nabla u(\mathbf{x}) \tag{3}$$

where $u : \Omega \to \mathbb{R}$ = the electric potential, $\sigma : \Omega \to \mathcal{M}_{3\times3}(\mathbb{R})$ = the anisotropic electric conductivity, $\mathbf{E} : \Omega \to \mathbb{R}^3$ = the electric field and $\mathbf{J} : \Omega \to \mathbb{R}^3$ = the electric current density. Once u is solved for in equation (1), $\mathbf{E}$ and $\mathbf{J}$ can easily be found. These equations are commonly used to model electrostatics so they will be used by most (if not all) tDCs models. Since there is no unique solution to equation (1) additional restrictions are required.

1.2.2 The electrodes

A suitable restriction is one which models the electrodes. Many simple boundary conditions such as specifying the electric current or potential at the surface of the scalp do not model the electrodes very accurately. This is shown in Somersalo's investigation [2].

Somersalo shows by comparison to an experiment that the 'complete electrode boundary condition', shown in equation (4), is the most accurate condition, assuming the electrodes are perfectly conductive. Somersalo also gives an interesting description into why this boundary condition is more accurate than the others.

From now on, let $\partial\Omega \subset \Omega$ be the boundary of Ω the patient's head; $\mathbf{x}_B \in \partial\Omega$ be some point on the boundary; $\hat{n} : \partial\Omega \to \mathbb{R}^3$ be the surface normal of $\partial\Omega$ the boundary; N be the total number of electrodes, $e(\gamma) \subset \partial\Omega$ be the closed, connected subset of the boundary that represents the part of the boundary that the γ'th electrode covers; and let $U(\gamma) \in \mathbb{R}$, $I(\gamma) \in \mathbb{R}$ and $z(\gamma) \in \mathbb{R}^+$ be the electric potential, electric current and the scalp-electrode impedance of the γ'th electrode respectively. The complete boundary condition is

$$-\mathbf{J}(\mathbf{x}_B)\cdot\hat{n}(\mathbf{x}_B) = \begin{cases} \frac{U(\gamma)-u(\mathbf{x}_B)}{z(\gamma)} & \mathbf{x}_B \in e(\gamma)\ \forall\,\gamma \in \{1,2,...,N\} \\ 0 & \text{otherwise} \end{cases} \tag{4}$$

where the current flowing through an electrode is given by

$$I(\gamma) = -\int\limits_{\mathbf{x}\in e(\gamma)} \mathbf{J}(\mathbf{x})\cdot\hat{n}(\mathbf{x})\,d\mathbf{x} \tag{5}$$

This boundary condition is classed as a robin boundary condition. Given $I(\gamma)$ and $z(\gamma)$, Somersalo shows that a multi-dimensional, variational technique can be used to find the solution to u and U that satisfies the boundary condition.

1.3 Solutions to tDCs models

Solutions to other models of tDCs already exist [3] however these models do not use the complete boundary condition. An effort is currently being made to produce solutions to an accurate tDCs model using the complete electrode boundary condition described in equation (4).

To model the detailed geometry of the head and the detailed changes in conductivity in different parts of the head, a numerical solution to the model with the complete boundary conditions is being developed where Ω and σ are not constrained.

To test this numerical model for accurateness, an analytic solution to the model has been developed by my supervisor, Prof. Peter Johnston, where Ω the shape of the head is constrained to a sphere and σ the electrical conductivity is constrained to be constant in spherical 'shells'. These constraints make it simple enough to solve equation (1) completely analytically and equation (4) almost completely analytically with a few integrals evaluated numerically.

The sphere has many symmetries that are not present in a human head and does not represent the shape of the human head very closely. To produce an analytical model that removes some of the symmetries of the sphere and better represents the shape of the human head, my AMSI vacation research scholarship project was to generalize the spherical solution to a prolate spheroidal [1] solution. This solution will be used to confirm the accuracy of the analytic spherical solution and the numerical solution.

2 Method

2.1 An analytic prolate spheroidal model of tDCs

In the analytic prolate spheroidal solution with the complete electrode boundary conditions, Ω the shape of the head is constrained to a prolate spheroid and σ the electrical conductivity is constrained to be constant in prolate spheroidal 'shells'.

The model becomes much easier to solve using a prolate spheroidal co-ordinate transformation. Let $\underline{\mathbf{x}} = (\xi, \theta, \phi)$ be the co-ordinates of the transformation, t, such that

$$t : \underline{\Omega} \to \Omega \; ; \; \mathbf{x} = t(\underline{\mathbf{x}}) = \begin{pmatrix} c\sqrt{\xi^2 - 1}\sin(\theta)\cos(\phi) \\ c\sqrt{\xi^2 - 1}\sin(\theta)\sin(\phi) \\ c\xi\cos(\theta) \end{pmatrix} \tag{6}$$

[1] A prolate spheroid is a 3-d surface produced by the rotation of an ellipse about the semi-major axis.

[4] Where $\underline{\Omega}$ is the space that represents the head using the prolate spheroidal co-ordinates, $\xi \in [1, \infty], \theta \in [0, \pi], \phi \in [0, 2\pi) \implies \underline{\Omega} \subset [1, \infty) \times [0, \pi] \times [0, 2\pi)$ and c is a parameter that is intended to remain constant.

To make equation (4) easier to solve for, $\underline{\Omega}$ will be restricted to a rectangular prism in the prolate spheroidal co-ordinates where

$$\underline{\Omega} = [1, \xi_0] \times [0, \pi] \times [0, 2\pi) \tag{7}$$

so that the shape of the head in Euclidean space Ω becomes a prolate spheroid. ξ_0 is the ξ co-ordinate whose co-ordinate surface is the boundary of the head. This means that the boundary of the head in prolate spheroidal co-ordinates is simply $\underline{\partial\Omega} = \{\xi_0\} \times [0, \pi] \times [0, 2\pi)$.

To make equation (4) slightly easier to solve the shape of the electrodes will be restricted to be rectangular in the prolate spheroidal co-ordinate system. Let the area that the γ'th electrode is placed on be represented in prolate spheroidal co-ordinates as $\underline{e}(\gamma) \subset \underline{\partial\Omega}$ such that $e(\gamma) = t(\underline{e}(\gamma))$,[2]. Since $\underline{\partial\Omega}$ is so simple, $\underline{e}(\gamma)$ is restricted as a rectangle simply by

$$\underline{e}(\gamma) = \{\xi_0\} \times [e_1(\gamma), e_2(\gamma)] \times [e_3(\gamma), e_4(\gamma)] \tag{8}$$

where $e_1(\gamma), e_2(\gamma) \in [0, \pi]$ and $e_3(\gamma), e_4(\gamma) \in [0, 2\pi]$ describe the edges of the electrode rectangles. This restriction could be removed without adding too much additional complexity to the solution but may make it more difficult to numerically evaluate the solution.

To make equation (1) easier to solve for, $\sigma(\underline{\mathbf{x}})$ will be restricted to be piecewise constant, only varying with the ξ co-ordinate such that

$$\sigma(\underline{\mathbf{x}}) = \begin{cases} \epsilon(n) & : \xi_S(n-1) \leq \xi < \xi_S(n) \; \forall \; n \in \{1, 2, ..., R-1\} \\ \epsilon(R) & : \xi_S(R-1) \leq \xi \leq \xi_S(R) \end{cases} \tag{9}$$

where $\epsilon(n)$ is the electrical conductivity of the n'th layer, R is the total number of layers and ξ_S is the series of ξ co-ordinates that are the boundaries of the layers such that $1 = \xi_S(0)$, $\xi_S(n-1) < \xi_S(n)$ and $\xi_S(R) = \xi_0$. This is a reasonable restriction in terms of modelling the human head as it represents the different layers of the head such as the scalp, skull, cerebral spinal fluid and the brain.

[2]Here $t(a)$ where a is a set, is the image of a under the function t.

Let $\underline{\xi}$, $\underline{\theta}$ and $\underline{\phi}$ be the co-ordinate vectors of the co-ordinates ξ, θ and ϕ. To once again make equation (1) easier to solve for, $\epsilon(n)$ is restricted in such a way that

$$\begin{aligned} \epsilon(n)\underline{\xi} &= \epsilon_r(n)\underline{\xi} \\ \epsilon(n)\underline{\theta} &= \epsilon_\perp(n)\underline{\theta} \\ \epsilon(n)\underline{\phi} &= \epsilon_\perp(n)\underline{\phi} \end{aligned} \tag{10}$$

where $\epsilon_r(n) \in \mathbb{R}^+$ and $\epsilon_\perp(n) \in \mathbb{R}^+$. This is a reasonable restriction as-well because the skull has been shown experimentally to have a greater conductivity tangential to the skull surface than normal to the skull surface. The other parts of the head will be approximated as isotropic.

2.2 Finding a solution to the model

In this model $I(\gamma)$, $z(\gamma)$, σ, c, ξ_0 and $e(\gamma)$ are assumed to be known and given. The electric potential u and the electric potential of the electrodes $U(\gamma)$ is the solution to the model where $\mathbf{E}$ and $\mathbf{J}$ can easily then be obtained from u. The solution to the problem can be found by first finding all possible u that satisfy equation (1) and then out of these possible u, finding the u and U that satisfy equation (4). Somersalo [2] has shown that there is only one unique solution that satisfies both equations.

2.2.1 Finding a solution to equation (1)

Equation (1) is restated in equation (11) using the prolate spheroidal co-ordinates, $\underline{\mathbf{x}}$.

$$\nabla \cdot \sigma(\underline{\mathbf{x}})\nabla u(\underline{\mathbf{x}}) = 0 \tag{11}$$

If

$$u(\underline{\mathbf{x}}) = \begin{cases} u(\underline{\mathbf{x}}, n) & : \xi_S(n-1) \leq \xi < \xi_S(n) \; \forall \; n \in \{1, 2, ..., R-1\} \\ u(\underline{\mathbf{x}}, R) & : \xi_S(R-1) \leq \xi \leq \xi_S(R) \end{cases} \tag{12}$$

then for $\xi_S(n-1) < \xi < \xi_S(n)$, equation (11) becomes

$$\nabla \cdot \epsilon(n)\nabla u(\underline{\mathbf{x}}, n) = 0 \tag{13}$$

To satisfy equation (11), the function $\sigma(\underline{\mathbf{x}})\nabla u(\underline{\mathbf{x}})$ must be continuous for all $\underline{\mathbf{x}} \in \underline{\Omega}$. Additionally the derivation of equation (1) requires that $\nabla u(\mathbf{x})$ be finite and therefore $u(\underline{\mathbf{x}})$ must be continuous. So assuming that $u(\underline{\mathbf{x}}, n)$ satisfies both these conditions then it is only necessary to state that

$$\lim_{\xi \to \xi_S(n)^-} u(\underline{\mathbf{x}}, n-1) = \lim_{\xi \to \xi_S(n)^+} u(\underline{\mathbf{x}}, n) \; \forall \; n \in \{1, 2, ..., R-1\} \tag{14}$$

$$\lim_{\xi\to\xi_S(n)^-}\epsilon(n-1)\nabla u(\underline{\mathbf{x}},n-1)=\lim_{\xi\to\xi_S(n)^+}\epsilon(n)\nabla u(\underline{\mathbf{x}},n)\ \forall\ n\in\{1,2,...,R-1\} \tag{15}$$

So equations (13,14,15) are equivelent to equation (11) over the whole domain $\underline{\Omega}$.

Assuming that $u(\underline{\mathbf{x}},n)$ is at least twice differentiable,

$$\begin{array}{c}\nabla\cdot\epsilon(n)\nabla u(\underline{\mathbf{x}},n)=\frac{1}{c^2(\xi^2-\cos^2(\theta))}\left[\epsilon_r(n)\frac{\partial}{\partial\xi}\left((\xi^2-1)\frac{\partial u}{\partial\xi}\right)+\right.\\ \left.\frac{\epsilon_\perp(n)}{\sin(\theta)}\frac{\partial}{\partial\theta}\left(\sin(\theta)\frac{\partial u}{\partial\theta}\right)+\epsilon_\perp(n)\left[\frac{1}{\sin^2(\theta)}+\frac{1}{\xi^2-1}\right]\frac{\partial}{\partial\phi}\left(\frac{\partial u}{\partial\phi}\right)\right]=0\end{array} \tag{16}$$

which shows that

$$\left[\frac{\epsilon_r(n)}{\epsilon_\perp(n)}\frac{\partial}{\partial\xi}\left((\xi^2-1)\frac{\partial u}{\partial\xi}\right)+\frac{1}{\sin(\theta)}\frac{\partial}{\partial\theta}\left(\sin(\theta)\frac{\partial u}{\partial\theta}\right)+\left[\frac{1}{\sin^2(\theta)}+\frac{1}{\xi^2-1}\right]\frac{\partial}{\partial\phi}\left(\frac{\partial u}{\partial\phi}\right)\right]=0 \tag{17}$$

By seeking a solution of the form

$$u(\underline{\mathbf{x}},n)=\Xi(\xi,n)\times\Theta(\theta)\times\Phi(\phi) \tag{18}$$

equation (17) can be separated into the three ODEs

$$\frac{\epsilon_r(n)}{\epsilon_\perp(n)\times\Xi(\xi,n)}\frac{\partial}{\partial\xi}\left((\xi^2-1)\frac{\partial\Xi}{\partial\xi}(\xi,n)\right)-C_1\frac{1}{\xi^2-1}=C_2 \tag{19}$$

$$\frac{1}{\sin(\theta)\times\Theta(\theta)}\frac{\partial}{\partial\theta}\left(\sin(\theta)\frac{\partial\Theta}{\partial\theta}(\theta)\right)-C_1\frac{1}{\sin^2(\theta)}=-C_2 \tag{20}$$

$$\frac{1}{\Phi(\phi)}\left(\frac{\partial^2\Phi}{\partial\phi^2}(\phi)\right)=-C_1 \tag{21}$$

where $C_1,C_2\in\mathbb{R}$ are real constants. Equations (19,20) are associated Legendre differential equations and equation (21) is a simple ODE. Since the co-ordinate transformation used is periodic in the ϕ co-ordinate with a periodicity of 2π, the solution to equation (21) is

$$\Phi(\phi)=\sum_{a=0}^{1}C_3(a)\begin{cases}\sin(k\phi) & :\ a=0\\ \cos(k\phi) & :\ a=1\end{cases} \tag{22}$$

where $C_1=k^2$ and $C_3(a)$ is some constant dependant on a.

If $C_2=l(l+1)$ where $l\in\mathbb{R}$ (Assuming that $C_2>-1/4$) then the solution to equation (20) is the associated Legendre function of the first and second kind $\Theta(\theta)=C_4P_l^k\left(\cos(\theta)\right)+C_5Q_l^k\left(\cos(\theta)\right)$ where P_l^k and Q_l^k are the associated Legendre functions

of the first and second kind with degree k and order l. To ensure that u is finite for all $\theta \in [0, \pi]$, $C_5 = 0$, $l \in \mathbb{Z}^+$ and $k \in \{0, 1, ..., l\}$ so the solution to equation (20) is

$$\Theta(\theta) = C_4 P_l^k(\cos(\theta)) \tag{23}$$

Equation (19) can be solved in a similar way. If $a(n) = \epsilon_\perp(n)/\epsilon_r(n)$, $\mu(k,n) = k\sqrt{a(n)}$ and $\lambda(l,n) = \sqrt{a(n)l(l+1) + \frac{1}{4}} - \frac{1}{2}$, then the solution to equation (19) is

$$\Xi(\xi, n) = \sum_{b=0}^{1} C_6(b,n) \begin{cases} P_{\lambda(l,n)}^{\mu(k,n)}(\xi) & : \ b = 0 \\ Q_{\lambda(l,n)}^{\mu(k,n)}(\xi) & : \ b = 1 \end{cases} \tag{24}$$

To ensure that u is finite when $\xi = 1$, $C_6(1,1) = 0$.

By using equations (14,15) and after some algebra, it can be shown that the constants $C_6(b,n)$ are related by

$$C_6(b,n) = C_6(0,1)\beta(b,n) \tag{25}$$

where $C_6(0,1)$ is the only unknown and $\beta(b,n)$ is determined by the following recursion relation

$$\boldsymbol{\alpha}(n) \begin{pmatrix} \beta(0,n) \\ \beta(1,n) \end{pmatrix} = \begin{pmatrix} \beta(0,n+1) \\ \beta(1,n+1) \end{pmatrix} \tag{26}$$

$$\begin{pmatrix} \beta(0,1) \\ \beta(1,1) \end{pmatrix} = \begin{pmatrix} 1 \\ 0 \end{pmatrix} \tag{27}$$

$$\boldsymbol{\alpha}(n) = \begin{cases} \begin{pmatrix} 1 & 0 \\ 0 & 0 \end{pmatrix} & : \ l = k = 0 \\ \begin{pmatrix} \frac{\left(\frac{b_1}{b_4} - \frac{c_1}{c_4}\right)}{\left(\frac{b_3}{b_4} - \frac{c_3}{c_4}\right)} & \frac{\left(\frac{b_2}{b_4} - \frac{c_2}{c_4}\right)}{\left(\frac{b_3}{b_4} - \frac{c_3}{c_4}\right)} \\ \frac{\left(\frac{b_1}{b_3} - \frac{c_1}{c_3}\right)}{\left(\frac{b_4}{b_3} - \frac{c_4}{c_3}\right)} & \frac{\left(\frac{b_2}{b_3} - \frac{c_2}{c_3}\right)}{\left(\frac{b_4}{b_3} - \frac{c_4}{c_3}\right)} \end{pmatrix} & : \text{ otherwise} \end{cases} \tag{28}$$

where:

$$\begin{array}{l|l} b_1 = \epsilon_r(n) \frac{dP_{\lambda(l,n)}^{\mu(k,n)}(\xi)}{d\xi}(\xi_S(n)) & c_1 = P_{\lambda(l,n)}^{\mu(k,n)}(\xi_S(n)) \\ b_2 = \epsilon_r(n) \frac{dQ_{\lambda(l,n)}^{\mu(k,n)}(\xi)}{d\xi}(\xi_S(n)) & c_2 = Q_{\lambda(l,n)}^{\mu(k,n)}(\xi_S(n)) \\ b_3 = \epsilon_r(n+1) \frac{dP_{\lambda(l,n+1)}^{\mu(k,n+1)}(\xi)}{d\xi}(\xi_S(n)) & c_3 = P_{\lambda(l,n+1)}^{\mu(k,n+1)}(\xi_S(n)) \\ b_4 = \epsilon_r(n+1) \frac{dQ_{\lambda(l,n+1)}^{\mu(k,n+1)}(\xi)}{d\xi}(\xi_S(n)) & c_4 = Q_{\lambda(l,n+1)}^{\mu(k,n+1)}(\xi_S(n)) \end{array} \tag{29}$$

Postal Address: 111 Barry Street
c/- The University of Melbourne
Victoria 3010 Australia

Email: enquiries@amsi.org.au
Phone: +61 3 8344 1777
Fax: +61 3 9349 4106
Web: www.amsi.org.au

So finally by using all the previous results, and using the fact that the gradient and divergence operators are linear, the general solution to equation (11) is

$$u(\underline{\mathbf{x}}) = \sum_{l=0}^{\infty} \sum_{k=0}^{l} \sum_{a=\delta(k,0)}^{1} C(l,k,a) \times \Xi(\xi,l,k) \times \Theta(\theta,l,k) \times \Phi(\phi,k,a) \tag{30}$$

where $C(a) = C_6(1,0) \times C_4 \times C_3(a)$ and $a = 0$ is not summed over when $k = 0$ because $\Phi(\phi,0,0) = 0$ and therefore $C(l,0,0)$ is arbitrary and the solution would be overdetermined. Ξ, Θ and Φ are defined as

$$\Phi(\phi,k,a) = \frac{1}{\sqrt{\pi}} \begin{cases} \sin(k\phi) & : \ a = 0 \\ \cos(k\phi) & : \ a = 1 \end{cases} \tag{31}$$

$$\Theta(\theta,l,k) = \sqrt{\frac{(2l+1)\,(l-k)!}{2\,(l+k)!}} P_l^k\left(\cos(\theta)\right) \tag{32}$$

$$\Xi(\xi,l,k) = w(l,k) \times \sum_{b=0}^{1} \begin{cases} \Xi(\xi,l,k,b,1) & : \ \xi_S(n-1) \le \xi < \xi_S(n) \,\forall\, n \in \{1,2,...,R-1\} \\ \Xi(\xi,l,k,b,R) & : \ \xi_S(R-1) \le \xi \le \xi_S(R)) \end{cases} \tag{33}$$

$$\Xi(\xi,l,k,b,n) = \beta(l,k,b,n) \begin{cases} P_{\lambda(l,n)}^{\mu(k,n)}(\xi) & : \ b = 0 \\ Q_{\lambda(l,n)}^{\mu(k,n)}(\xi) & : \ b = 1 \end{cases} \tag{34}$$

where the functions Ξ, Θ and Φ have been normalized over the domain $\underline{\Omega}$ to avoid round-off errors and overflows in the numerical evaluation of the solution. The normalizing constants $w(l,k)$ are evaluated to satisfy $\int_1^{\xi_0} \left(\Xi(\xi,l,k)\right)^2 d\xi = 1$ for all l and k.

2.2.2 Finding a solution to the boundary condition (4)

To solve the boundary condition, shown in equation (4), a multi-dimensional variational technique must be used which results in a quadratic functional which is minimized by the solution to the boundary condition. Thankfully Somersalo [2] has shown the quadratic functional, f, in equation (35) is minimized by the solution to this model.

$$f(u,U) = \frac{1}{2} \int_{\Omega} (\sigma(\boldsymbol{x}) \nabla u(\boldsymbol{x})) \cdot (\nabla u(\boldsymbol{x}))\, dV + \frac{1}{2} \sum_{\gamma=1}^{N} \frac{1}{z(\gamma)} \int_{e(\gamma)} |u(\boldsymbol{x}) - U(\gamma)|^2\, dS - \sum_{\gamma=1}^{N} I(\gamma) U(\gamma) \tag{35}$$

It's worth mentioning that Sommersalo let $\sigma \in \mathbb{C}$ and it's been assumed that generalizing this to $\sigma \in \mathcal{M}_{3\times 3}(\mathbb{R})$ still leads to the quadratic functional in equation (35).

By substituting the function u in equation (35) into the functional f and after a considerable amount of algebra the quadratic functional becomes the quadratic function in equation (36)

$$f(C,U) = \frac{1}{2}\sum_{l=0}^{\infty}\sum_{l'=0}^{\infty}\sum_{k=0}^{l}\sum_{k'=0}^{l'}\sum_{a=\delta(k,0)}^{1}\sum_{a'=\delta(k',0)}^{1}\delta(k,k')\times\delta(a,a')\times C(l,k,a)\times C(l',k,a)\times\eta_1(l,l',k,a)+$$

$$\sum_{l=0}^{\infty}\sum_{l'=0}^{\infty}\sum_{k=0}^{l}\sum_{k'=0}^{l}\sum_{a=\delta(k,0)}^{1}\sum_{a'=\delta(k,0)}^{1}C(l,k,a)\times C(l',k',a')\times\frac{1}{2}c^2\sqrt{(\xi_0^2-1)}\times\eta_2(l,l',k,k',a,a')- \tag{36}$$

$$c^2\sqrt{(\xi_0^2-1)}\left(\sum_{\gamma=1}^{N}\sum_{l=0}^{\infty}\sum_{k=0}^{l}\sum_{a=\delta(k,0)}^{1}U(\gamma)\times C(l,k,a)\times\eta_3(\gamma,l,k,a)\right)+\frac{1}{2}c^2\sqrt{(\xi_0^2-1)}\sum_{\gamma=1}^{N}U(\gamma)^2\times\eta_4(\gamma)-\sum_{\gamma=1}^{N}I(\gamma)U(\gamma)$$

where

$$\eta_1(l,l',k,a) = \delta(l,l')\times\left[\int_{\xi=1}^{\xi_0}\sigma_r(\xi)\left(\frac{d\Xi}{d\xi}(\xi,l,k)\right)^2(\xi^2-1)\,d\xi + k^2\times\int_{\xi=1}^{\xi_0}\left(\frac{\sigma_\perp(\xi)}{(\xi^2-1)}\Xi(\xi,l,k)\times\Xi(\xi,l,k)\right)d\xi\right]+$$

$$\int_{\xi=1}^{\xi_0}\left(\sigma_\perp(\xi)\times\Xi(\xi,l,k)\times\Xi(\xi,l',k)\right)d\xi\times\left[\int_{\theta=0}^{\pi}\left(\frac{d\Theta}{d\theta}(\theta,l,k)\times\frac{d\Theta}{d\theta}(\theta,l',k)\right)\sin(\theta)d\theta + k^2\times\int_{\theta=0}^{\pi}\Theta(\theta,l,k)\times\Theta(\theta,l',k)\frac{d\theta}{\sin(\theta)}\right] \tag{37}$$

$$\eta_2(l,l',k,k',a,a') = \Xi(\xi_0,l,k)\times\Xi(\xi_0,l',k')\times\sum_{\gamma=1}^{N}\left[\frac{1}{z(\gamma)}\times\int_{\theta=e_1(\gamma)}^{e_2(\gamma)}\left(\sin(\theta)\sqrt{(\xi_0^2-\cos^2(\theta))}\Theta(\theta,l,k)\times\Theta(\theta,l',k')\right)d\theta\times\right.$$

$$\left.\int_{\phi=e_3(\gamma)}^{e_4(\gamma)}\left(\Phi(\phi,k,a)\times\Phi(\phi,k',a')\right)d\phi\right] \tag{38}$$

$$\eta_3(\gamma,l,k,a) = \Xi(\xi_0,l,k)\times\frac{1}{z(\gamma)}\int_{\theta=e_1(\gamma)}^{e_2(\gamma)}\left(\sin(\theta)\sqrt{(\xi_0^2-\cos^2(\theta))}\Theta(\theta,l,k)\right)d\theta\times\int_{\phi=e_3(\gamma)}^{e_4(\gamma)}\left(\Phi(\phi,k,a)\right)d\phi \tag{39}$$

$$\eta_4(\gamma) = \frac{1}{z(\gamma)}\left(e_4(\gamma)-e_3(\gamma)\right)\int_{\theta=e_1(\gamma)}^{e_2(\gamma)}\sin(\theta)\sqrt{(\xi_0^2-\cos^2(\theta))}d\theta \tag{40}$$

where $\sigma_r(\xi) = \epsilon_r(n) : \xi_S(n-1) \le \xi < \xi_S(n)$, $\sigma_\perp(\xi) = \epsilon_\perp(n) : \xi_S(n-1) \le \xi < \xi_S(n)$ and many of the integrals in (37-40) are evaluated analytically which is shown in Appendix 1.

The expression for the quadratic function is very difficult to deal with but since it is a quadratic function of the unknowns $U(\gamma)$ and $C(l,k,a)$, the expression can be creatively put into a compact vector and matrix form. Let $\boldsymbol{y} = (y(j))_{0\le j<\infty}$ and

$$y(j) = U(j+1)\ :\ 0 \le j \le N-1 \tag{41}$$

$$y(j) = C(l,k,a) \ : \ j \geq N \ ; \ j = N + l^2 + 2k + a - 1 \tag{42}$$

Also let $\boldsymbol{r} = (r(j))_{0 \leq j < \infty}$ and

$$r(j) = \begin{cases} I(j+1) & : \ 0 \leq j \leq N-1 \\ 0 & \text{otherwise} \end{cases} \tag{43}$$

By substituting $y(j)$ for $U(\gamma)$ and $C(l,k,a)$ and $r(j)$ for $I(\gamma)$ in equation (36), the quadratic function f can be expressed as the following very compact form

$$f(\boldsymbol{y}) = \boldsymbol{y}^T \boldsymbol{S} \boldsymbol{y} - \boldsymbol{y}^T \boldsymbol{r} \tag{44}$$

where

$$\boldsymbol{S} = \begin{pmatrix} \boldsymbol{S}_1 & \boldsymbol{S}_2 \\ \boldsymbol{S}_3 & \boldsymbol{S}_4 \end{pmatrix} \tag{45}$$

$$\boldsymbol{S}_1 = \frac{1}{2} c^2 \sqrt{(\xi_0^2 - 1)} \left(\delta(j,j') \times \eta_4(j+1) \right) \quad \begin{matrix} 0 \leq j < N \\ 0 \leq j' < N \end{matrix} \tag{46}$$

$$\boldsymbol{S}_2 = -\frac{1}{2} c^2 \sqrt{(\xi_0^2 - 1)} \left(\eta_3(j'+1,l,k,a) \right) \quad \begin{matrix} N \leq j < \infty \\ 0 \leq j' < N \end{matrix} \tag{47}$$

$$\boldsymbol{S}_3 = -\frac{1}{2} c^2 \sqrt{(\xi_0^2 - 1)} \left(\eta_3(j+1,l',k',a') \right) \quad \begin{matrix} 0 \leq j < N \\ N \leq j' < \infty \end{matrix} \tag{48}$$

$$\boldsymbol{S}_4 = \frac{1}{2} \left(c \times \delta(k,k') \times \delta(a,a') \times \eta_1(l,l',k,a) + c^2 \sqrt{(\xi_0^2 - 1)} \times \eta_2(l,l',k,k',a,a') \right) \quad \begin{matrix} N \leq j < \infty \\ N \leq j' < \infty \end{matrix} \tag{49}$$

Where the indexing used the relations $j = N + l^2 + 2k + a - 1$ and $j' = N + l'^2 + 2k' + a' - 1$.

To find the solution to the model, f must be minimized. This could be done by setting the gradient of f equal to the zero vector or equivalently the derivative of f w.r.t $\boldsymbol{y}$ could be set to the zero vector. The equations (50,51) show that the expression for $\boldsymbol{y}$ in equation (52) gives the minimum value for f.

$$\frac{df}{d\boldsymbol{y}} = \lim_{\delta \boldsymbol{y} \to 0} (\delta \boldsymbol{y})^{-1} \left[f(\boldsymbol{y} + \delta \boldsymbol{y}) - f(\boldsymbol{y}) \right] \tag{50}$$

where $(\delta \boldsymbol{y})^{-1} \cdot \delta \boldsymbol{y} = 1$ and by substituting f into (50) it can be shown that

$$\frac{df}{d\boldsymbol{y}} = 2\boldsymbol{S}\boldsymbol{y} - \boldsymbol{r} \tag{51}$$

By setting the derivative to the zero vector, the value of $\mathbf{y}$ that minimizes f and therefore is the solution to the model is given by

$$\boldsymbol{y} = \frac{1}{2}\boldsymbol{S}^{-1}\boldsymbol{r} \tag{52}$$

2.3 Numerical evaluation of the solution

The matrix $\boldsymbol{S}$ and it's inverse are too difficult to completely evaluate analytically and therefore the solution must be numerically evaluated. However since the matrix $\boldsymbol{S}$ has an infinite size, it cannot be numerically evaluated.

To find an approximation to the solution that can be numerically evaluated, $\mathbf{y}$ & $\boldsymbol{S}$ has to be truncated to a finite size. Let the potential function u be approximated by only summing the first $L+1$ terms of the $\sum_{l=0}^{\infty}$ sum so that the approximation to u, labelled u_T is given by

$$u_T(\underline{\mathbf{x}}) = \sum_{l=0}^{L} \sum_{k=0}^{l} \sum_{a=\delta(k,0)}^{1} C(l,k,a) \times \Xi(\xi,l,k) \times \Theta(\theta,l,k) \times \Phi(\phi,k,a) \tag{53}$$

Clearly $u = u_T + \delta u$ where δu is the error in the approximation and since the series in (30) is convergent, as $L \to \infty$, $u_T \to u$ and therefore $\delta u \to 0$.

To numerically evaluate the solution a Python3 program was developed which was run on a computer using double precision floating point arithmetic. The SciPy and NumPy Python3 libraries were used to numerically evaluate the integrals using an adaptive Gaussian quadrature algorithm; evaluate the associated Legendre functions for integer degree and order; and perform matrix operations.

To evaluate the associated Legendre functions with non-integer degree and/or order the following relationships between the Legendre, gamma and Guass hypergeometric functions was used

$$P_{\lambda}^{\mu}(z) = \frac{1}{\Gamma(1-\mu)} \left[\frac{1+z}{1-z}\right]^{\mu/2} F(-\lambda, \lambda+1; 1-\mu; \frac{1-z}{2}) \tag{54}$$

$$Q_{\lambda}^{\mu}(z) = \frac{\sqrt{\pi}\Gamma(\lambda+\mu+1)}{2^{\lambda+1}\Gamma(\lambda+3/2)} \frac{e^{i\pi\mu}\,(z^2-1)^{\mu/2}}{z^{\lambda+\mu+1}} F\left(\frac{\lambda+\mu+1}{2}, \frac{\lambda+\mu+2}{2}; \lambda+\frac{3}{2}; \frac{1}{z^2}\right) \tag{55}$$

Where Γ's the gamma function and F is the guass hyper-geometric function.

Since the associated Legendre differential equation is linear and because the real and imaginary parts of $P_\lambda^\mu(z)$ and $Q_\lambda^\mu(z)$ are proportional, it can be shown that the following two functions are also solutions to the Legendre differential equation and are real for $z \geq 1$.

$$P_\lambda^\mu(z) = \frac{1}{\Gamma(1-\mu)} \left[\frac{1+z}{z-1}\right]^{\mu/2} F(-\lambda, \lambda+1; 1-\mu; \frac{1-z}{2}) \tag{56}$$

$$Q_\lambda^\mu(z) = \frac{\sqrt{\pi}\Gamma(\lambda+\mu+1)}{2^{\lambda+1}\Gamma(\lambda+3/2)} \frac{(z^2-1)^{\mu/2}}{z^{\lambda+\mu+1}} F\left(\frac{\lambda+\mu+1}{2}, \frac{\lambda+\mu+2}{2}; \lambda+\frac{3}{2}; \frac{1}{z^2}\right) \tag{57}$$

These slightly modified Legendre functions were used for the numerical evaluations because only a real solution is of interest.

2.4 Comparing the model

To compare the prolate spheroidal model with the spherical model the electrode potential $U(\gamma)$ was compared and the electric potential u was evaluated and compared at several points within the head. It can be shown that if α is the ratio between the semi-major and semi-minor axis lengths of the prolate spheroid then

$$\xi_0 = \sqrt{\frac{\alpha^2}{\alpha^2-1}} \tag{58}$$

which shows that as the prolate spheroid goes to a sphere ($\alpha \to 1^+$), then $\xi_0 \to \infty$ but $\alpha \neq 1$. By choosing a value for α close to 1, such as 1.00001 then the solution can be evaluated with no overflows or underflows and is very close to the spherical case. To compare the solution u at some point, u has to be evaluated in the spherical polar co-ordinates for the spherical model and then those co-ordinates must be transformed into prolate spheroidal co-ordinates so that u can be evaluated at the same point in the prolate spheroidal model. Let $g : \mathcal{C} \to \mathbb{R}^3$ be the co-ordinate transformation from spherical to Cartesian co-ordinates, then the transformation from spherical to prolate spheroidal co-ordinates is $t^{-1} \circ g$, [3]. This comparison was performed with a few different sets of parameters. These were

- A constant isotropic conductivity case.

[3] Here $a \circ b$, where a and b are functions, is the function composition operator such that $(a \circ b)(x) = a(b(x))$.

- An isotropic conductivity case with 4 layers that represent the human head.
- An anisotropic conductivity case with 4 layers that represent the human head.
- An anisotropic conductivity case with 4 layers where the conductivity change between layers is less dramatic.

3 Results and Discussion

3.1 Comparison to the analytic spherical model

3.1.1 Constant isotropic conductivity case

The case where the conductivity is constant through the whole head was the first comparison to be performed. This comparison shows that the two solutions give similar results that improve as $\alpha \to 1^+$. Table 1 shows the approximate average relative difference between the potential u given by the spherical model and the prolate spheroidal model.

Semi-major/minor	Rel. Error
1.01	$\approx 7 \times 10^{-3}$
1.005	$\approx 3 \times 10^{-3}$
1.0005	$\approx 3 \times 10^{-4}$
1.00005	$\approx 3 \times 10^{-5}$
1.000000005	$\approx 1 \times 10^{-7}$

Table 1: Convergence of the solution to the spherical model and the prolate spheroidal model.

This convergence was also present in the electrode potentials.

3.1.2 Isotropic conductivity with 4 layers of constant conductivity

The isotropic case with 4 layers of constant conductivity that represents the conductivity in the human head showed the same results as in section 3.1.1. Both the potential of the electrodes and the potential at the several test points within the head gave similar results with a relative error that converged to 0 as $\alpha \to 1^+$.

3.1.3 Anisotropic conductivity with 4 layers of constant conductivity

The anisotropic case with 4 layers of constant conductivity that represents the conductivity in the human head shows that the two models give different results in this case. With relative errors up to 0.5 in the potential at the test points within the head. However the relative error in the potential of the electrodes is only 5×10^{-6}.

As the conductivity of the anistropic layer (the skull) goes to the isotropic case, both models converge on the same solution.

3.1.4 Anistropic conductivity with 4 layers of constant conductivity 2

The anisotropic case with 4 layers of constant conductivity that don't change as dramatically shows that the two models give the same results. In this case the relative error of both the potential of the electrodes and the potential of the test points within the head go to zero as $\alpha \to 1^+$.

3.1.5 Discussion

Where the conductivity is isotropic the two models give very close results indicating that the differences are most likely only due to the error in the approximation of u and finite precision arithmetic errors. It also shows that many parts of the algebra in section 2.2 that do not concern the anisotropy of the conductivity is correct.

The first case where the conductivity is anisotropic shows that the models do not give the same results. However in the second case in section 3.1.2 where the conductivity does not vary as dramatically between the layers, the models do give the same results. The cause of this problem is still unknown. Some hypotheses for why the prolate spheroidal model may be inaccurate are listed below.

- The truncation size, L, that was used in the comparison may have been too low. For the anisotropic case, $L = 15$ was used because the numerical integration program reported excessive round-off error for $L > 15$.
- There may be some un-noticed, significant round-off error in the numerical evaluate in processes other than the numerical integration. One process where round-off error may be present is in the evaluation of $\boldsymbol{\alpha}$.
- The method that was used for evaluating the Legendre functions and their derivatives could be incorrect.

The last hypothesis could be tested by substituting the Legendre function and it's derivatives into the Legendre differential equation to test if the equality holds true.

To test if un-noticed round-off is present in the evaluation of $\boldsymbol{\alpha}$, the solution to u could be substituted into equations (14,15) and the equality could be tested numerically.

To test if the truncation size is too low, the solution could be evaluated for $L = 10, 11, ..., 14, 15$ to see if the truncated approximation is converging on the solution near $L = 15$, or if it is still varying dramatically.

Alternatively, arbitrary precision arithmetic methods could be used to reduce round-off error. By increasing the precision of the computer arithmetic L could be increased and it could be tested whether or not a low L value is to blame for the inaccuracy. By increasing the precision, the round-off errors present in all numerical processes will decrease which would test if there are any un-noticed significant round-off errors present.

3.2 Examples of use of the model (Investigation into electrode placements)

To demonstrate the use of the model, the model was used to investigate the electric potential and electric field produced by different electrode placements on the head.

The three electrode placements shown are some interesting examples of the use of the model each with different complexities and difficulties.

In these solutions to the model the truncation size used was $L = 15$, limited by round-off error and in the images the electric field is facing the opposite direction to the correct direction.

3.2.1 Electrode placement 1

In this electrode placement, two electrodes were approximately placed in the area where the human temples would be. Figure 1 shows a prolate spheroid with a colour map representing the electric potential on the surface of the head.

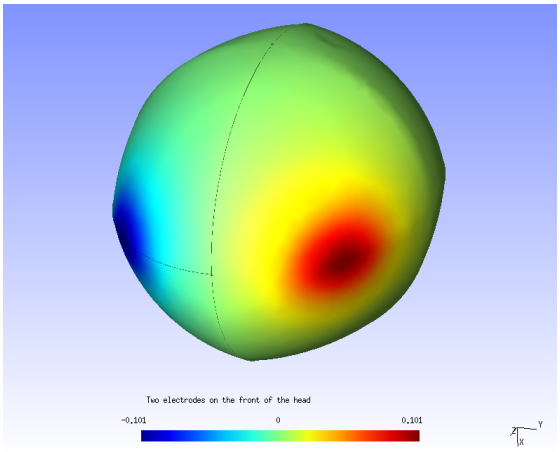

Figure 1: The electric potential on the surface of the head.

Since the electrodes are placed on a plane of symmetry some useful information about the electric potential and field can be obtained by viewing a cross section through this plane. Figure 2 shows the electric potential and electric field on this cross section. The electric potential is represented by a colour map and the electric field is represented by arrows where the colour and size of the arrow represents the magnitude of the electric field. Unfortunately the boundaries between the layers are not shown in the figure however there are clear changes in the electric field where the layers change. Due to the low truncation size, L=15, some irregularities can be seen in the electric field. This should be corrected if L is increased.

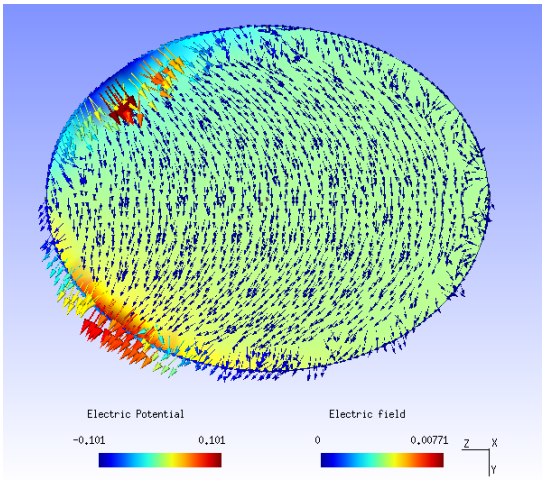

Figure 2: The electric potential and the electric field on the plane of symmetry.

The electric field inside the brain is of particular interest in tDCs. This can be observed in more detail by taking a higher resolution image of only the brain layer. This higher-resolution cross section is shown in Figure 3.

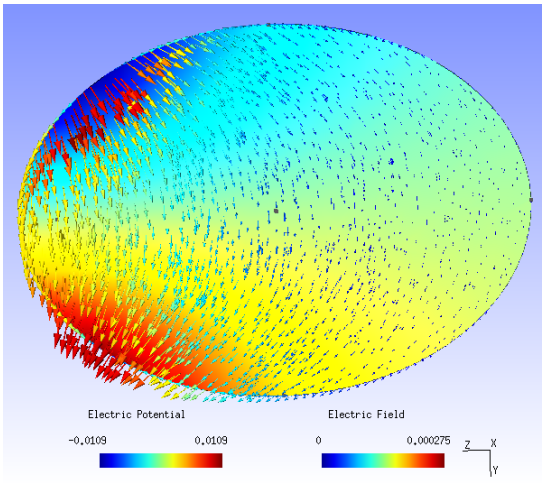

Figure 3: The electric potential and the electric field on the plane of symmetry for only the brain layer.

Figure 3 shows that the electric field due to this electrode configuration is strongest at the front of the brain and the direction of the field is mostly lateral.

Postal Address: 111 Barry Street
c/- The University of Melbourne
Victoria 3010 Australia

Email: enquiries@amsi.org.au
Phone: +61 3 8344 1777
Fax: +61 3 9349 4106
Web: www.amsi.org.au

3.2.2 Electrode placement 2

In this electrode placement two small electrodes have been placed on the temples of the head that sink current and one wide electrode has been placed along the top front of the head that source current. Figure 4 shows the electric potential on the surface of the head. This electrode configuration presents a challenge when trying to visualize

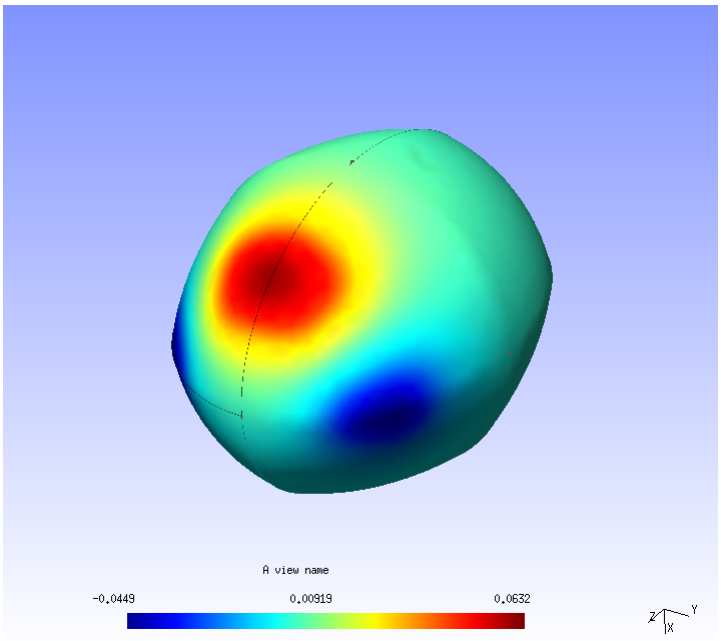

Figure 4: The electric potential on the surface of the head.

the solution as a static image because the electrodes don't lie on a plane of symmetry. Some information about the electric potential can be gained by viewing 3-d surfaces that have a common electric potential. Figure 5 illustrates the electric potential inside the brain for this electrode placement. The surfaces with a common colour share a common electric potential and therefore the electric field will be normal to these surfaces. The closer together the surfaces are the higher the electric field is in that area.

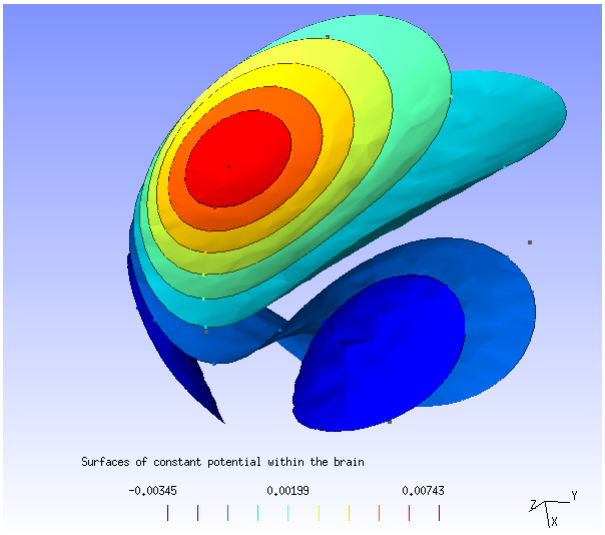

Figure 5: The electric potential inside the brain.

Figure 5 shows that the electric field produced by this electrode configuration is strongest directly underneath the large wide electrode.

3.2.3 Electrode placement 3

The final electrode configuration is a five electrode configuration where a central electrode sources current and 4 surround electrodes sink current. The goal in this particular electrode configuration was to observe how localized and how deep the highest part of the electric field would be in the brain. Figure 6 shows the electric potential on the surface of the head.

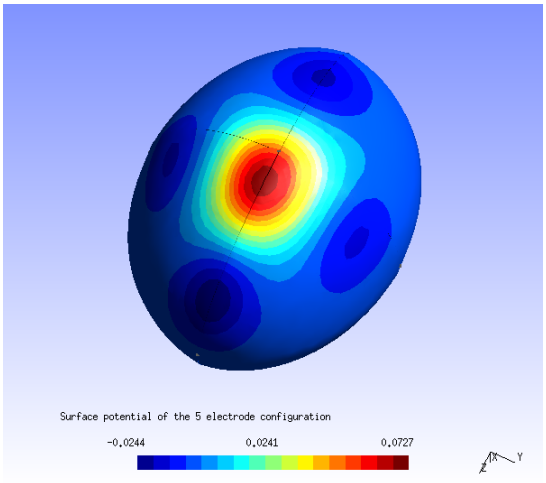

Figure 6: The electric potential on the surface of the head.

Since three of the electrodes are centred along a plane of symmetry, taking a cross section of the electric potential and field through this plane will give some information about the electric potential inside the head. Figure 7 shows this cross section through the head.

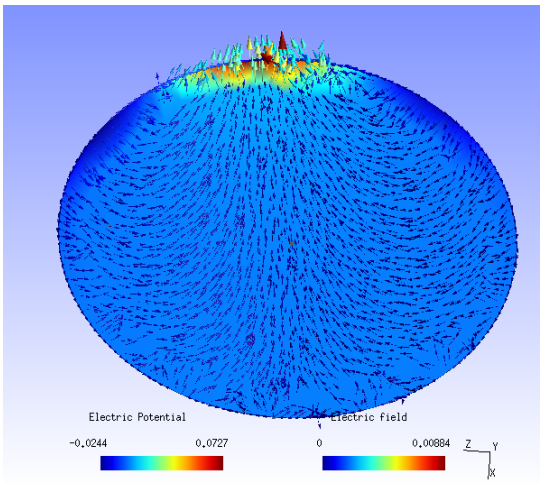

Figure 7: The electric potential and the electric field on the plane of symmetry.

Postal Address: 111 Barry Street
c/- The University of Melbourne
Victoria 3010 Australia

Email: enquiries@amsi.org.au
Phone: +61 3 8344 1777
Fax: +61 3 9349 4106
Web: www.amsi.org.au

This figure shows that the electric field under the central electrode is considerably higher than the electric field under the other electrodes. By once again taking a higher resolution image of only the brain layer, we get figure 8. This shows that the

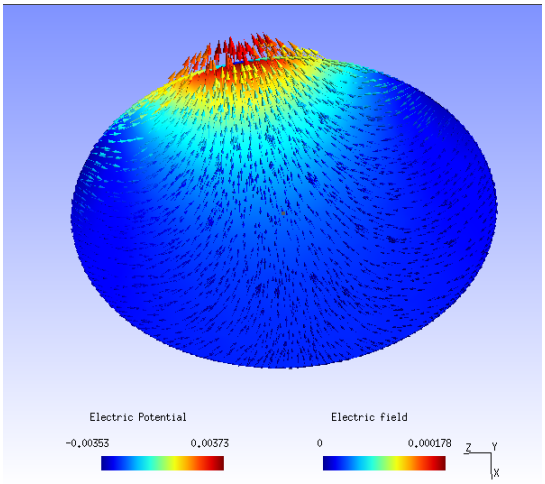

Figure 8: The electric potential and the electric field on the plane of symmetry for only the brain layer.

electric field is directed toward the central electrode in most parts of the brain and the amplitude of the electric field decreases as the distance from the central electrode increases. The depth of the affected volume is less than expected.

4 Conclusion

To assist the effort to create an accurate mathematical clinical tool for use in researching and using the transcranial direct current stimulation medical treatment, an analytical solution for a transcranial direct current stimulation model was found, evaluated and investigated. The mathematical model that was used, models the electric potential, field and current inside the human head using classical electromagnetism laws and uses a boundary condition that has been shown to accurately model electrodes. An analytic solution to this model that approximates the human head as a prolate spheroid with 'shells' of constant anisotropic conductivity has been developed to compare against a spherical, analytic solution and a general, numerical solution to the model to test the accuracy of the solutions.

The solution to the model where the shape of the head is restricted to a prolate spheroid can be mostly evaluated analytically using a prolate spheroidal co-ordinate transformation. Some integrals and matrix operations cannot practically be evaluated analytically and are required to be numerically evaluated to find the solution to the model. Additionally the solution must be approximated by truncating an infinite series to be numerically evaluated where the accuracy of the approximation is limited by the precision of the floating point arithmetic used and by the time taken to evaluate the solution.

When the prolate spheroidal solution is compared to the spherical solution, the solutions give the same results for some parameters to the model. In the case where the conductivity inside the head is isotropic, the two models give the same results for all parameters that have been tested. In the case where the conductivity is anisotropic, the two models only give the same results for some parameters. Hypotheses for why this is so have been discussed in section 3.1.5.

Finally a use of the model was demonstrated by using it to investigate the electric field inside a patients head produced by different electrode configurations.

5 Thanks and Acknowledgements

I'd like to thank and acknowledge my supervisor for all the help that I received in the AMSI VRS project and I'd like to thank AMSI for the opportunity and funding to complete this project.

References

[1] 2008, 'Transcranial direct current stimulation: State of the art 2008', 'BRAIN STIMULATION: Basic, Translational, and Clinical Research in Neuromodulation', Volume 1, Issue 3 , Pages 206-223

[2] Somersalo E, Cheney M & Isaacson D, 1992, 'Existence and Uniqueness for Electrode Models for Electric Current Computed Tomography', 'SIAM J. APPL. MATH' , Vol. 52, No. 4, pages 1023-1040

[3] Mirandaa P C, Lomarevb M& Hallettb M, 2006, 'Modeling the current distribution during transcranial direct current stimulation', 'Clinical Neurophysiology', Volume 117, Issue 7, Pages 1623-1629

[4] de Munck J C, 1988, 'The potential distribution in a layered anisotropic spheroidal volume conductor', 'J. Appl. Phys.' Vol. 64, Page 464

6 Appendix 1 - Analytic solutions for integrals in S

This appendix shows the analytic solutions to the integrals that appear in the η_1, η_2, η_3 and η_4 functions that are required to evaluate **S**.

Some integrals have only been evaluated for some special cases where or orthogonality relations can be used or the symmetry of the integrand within the domain of integration can be exploited to make it easy to evaluate.

Integrals that are not analytically evaluated are numerically integrated.

6.1 Integrals in η_1

For $l = l'$:

$$\int_{\theta=0}^{\pi} \Theta(\theta,l,k) \times \Theta(\theta,l',k) \frac{d\theta}{\sin(\theta)} = \int_{\theta=0}^{\pi} \Theta(\theta,l,k) \times \Theta(\theta,l,k) \frac{d\theta}{\sin(\theta)} = \frac{(2l+1)}{2k} \tag{59}$$

For l and l' not both even or both odd:

$$\int_{\theta=0}^{\pi} \Theta(\theta,l,k) \times \Theta(\theta,l',k) \frac{d\theta}{\sin(\theta)} = 0 \tag{60}$$

$$\int_{\theta=0}^{\pi} \left(\frac{d\Theta}{d\theta}(\theta,l,k) \times \frac{d\Theta}{d\theta}(\theta,l',k) \right) \sin(\theta) d\theta = 0 \tag{61}$$

The following integrals can be expanded to make numerical integration more accurate and faster.

$$\int_{\xi=1}^{\xi_0} \sigma_\xi(\xi) \left(\frac{d\Xi}{d\xi}(\xi,l,k) \right)^2 \left(\xi^2 - 1\right) d\xi =$$

$$\sum_{n=1}^{R} \epsilon_r(n) \sum_{b,b'=0}^{1} \int_{\xi=\xi_S(n-1)}^{\xi_S(n)} \left(w(l,k)\right)^2 \times \frac{d\Xi}{d\xi}(\xi,l,k,b,n) \times \frac{d\Xi}{d\xi}(\xi,l,k,b',n) \times \left(\xi^2 - 1\right) d\xi \tag{62}$$

Postal Address: 111 Barry Street
c/- The University of Melbourne
Victoria 3010 Australia

Email: enquiries@amsi.org.au
Phone: +61 3 8344 1777
Fax: +61 3 9349 4106
Web: www.amsi.org.au

$$\int_{\xi=1}^{\xi_0} \left(\frac{\sigma_\phi(\xi)}{(\xi^2-1)} \Xi(\xi,l,k) \times \Xi(\xi,l,k) \right) d\xi =$$

$$\sum_{n=1}^{R} \epsilon_\perp(n) \times \sum_{b,b'=0}^{1} \int_{\xi=\xi_S(n-1)}^{\xi_S(n)} \left(w(l,k)\right)^2 \times \left(\Xi(\xi,l,k,b,n) \times \Xi(\xi,l,k,b',n)\right) \frac{d\xi}{\xi^2-1} \quad (63)$$

$$\int_{\xi=1}^{\xi_0} \left(\sigma_\theta(\xi) \times \Xi(\xi,l,k) \times \Xi(\xi,l',k)\right) d\xi =$$

$$\sum_{n=1}^{R} \epsilon_\perp(n) \sum_{b,b'=0}^{1} \int_{\xi=\xi_S(n-1)}^{\xi_S(n)} w(l,k) \times w(l',k) \times \left(\Xi(\xi,l,k,b,n) \times \Xi(\xi,l',k,b',n)\right) d\xi \quad (64)$$

6.2 Integrals in η_2

$$\int_{\phi=e_3(\gamma)}^{e_4(\gamma)} \left(\Phi(\phi,k,a) \times \Phi(\phi,k',a')\right) d\phi =$$

$$= \frac{1}{2} \begin{cases} \frac{\sin((k-k')e_4(\gamma))-\sin((k-k')e_3(\gamma))}{(k-k')} - \frac{\sin((k+k')e_4(\gamma))-\sin((k+k')e_3(\gamma))}{(k+k')} & : k \neq k' \& a = a' = 0 \\ \left(e_4(\gamma)-e_3(\gamma)\right) - \frac{\sin((k+k')e_4(\gamma))-\sin((k+k')e_3(\gamma))}{(k+k')} & : k = k' \& a = a' = 0 \\ \frac{\sin((k-k')e_4(\gamma))-\sin((k-k')e_3(\gamma))}{(k-k')} + \frac{\sin((k+k')e_4(\gamma))-\sin((k+k')e_3(\gamma))}{(k+k')} & : k \neq k' \& a = a' = 1 \\ \left(e_4(\gamma)-e_3(\gamma)\right) + \frac{\sin((k+k')e_4(\gamma))-\sin((k+k')e_3(\gamma))}{(k+k')} & : k = k' \& a = a' = 1 \\ -\frac{\cos((k+k')e_4(\gamma))-\cos((k+k')e_3(\gamma))}{k+k'} - \frac{\cos((k-k')e_4(\gamma))-\cos((k-k')e_3(\gamma))}{k-k'} & : k \neq k' \& a = 0 \& a' = 1 \\ -\frac{\cos((k+k')e_4(\gamma))-\cos((k+k')e_3(\gamma))}{k+k'} & : k = k' \& a = 0 \& a' = 1 \\ -\frac{\cos((k+k')e_4(\gamma))-\cos((k+k')e_3(\gamma))}{k+k'} + \frac{\cos((k-k')e_4(\gamma))-\cos((k-k')e_3(\gamma))}{k-k'} & : k \neq k' \& a = 1 \& a' = 0 \\ -\frac{\cos((k+k')e_4(\gamma))-\cos((k+k')e_3(\gamma))}{k+k'} & : k = k' \& a = 1 \& a' = 0 \\ e_4(\gamma)-e_3(\gamma) & : k = k' = 0 \& a = a' = 1 \\ 0 & : k = k' = 0 \& a = a' = 0 \end{cases} \quad (65)$$

6.3 Integrals in η_3

$$\int_{\phi=e_3(\gamma)}^{e_4(\gamma)} \Phi(\phi,k,a)\,d\phi = \begin{cases} -\frac{1}{k}\left(\cos(ke_4(\gamma)) - \cos(ke_3(\gamma))\right) & : \ a=0; k\neq 0 \\ \frac{1}{k}\left(\sin(ke_4(\gamma)) - \sin(ke_3(\gamma))\right) & : \ a=1; k\neq 0 \\ e_4(\gamma) - e_3(\gamma) & : \ a=1; k=0 \end{cases} \tag{66}$$

6.4 Integrals in η_4

$$\int_{\theta=e_1(\gamma)}^{e_2(\gamma)} \sin(\theta)\sqrt{(\xi_0^2-\cos^2(\theta))}d\theta = -\frac{1}{2}\left[\cos(e_2(\gamma))\sqrt{\xi_0^2-\cos^2(e_2(\gamma))} - \right.$$

$$\left.\cos(e_1(\gamma))\sqrt{\xi_0^2-\cos^2(e_1(\gamma))} + \xi_0^2\left(\arcsin(\frac{\cos(e_2(\gamma))}{\xi_0}) - \arcsin(\frac{\cos(e_1(\gamma))}{\xi_0})\right)\right] \tag{67}$$

Postal Address: 111 Barry Street
c/- The University of Melbourne
Victoria 3010 Australia

Email: enquiries@amsi.org.au
Phone: +61 3 8344 1777
Fax: +61 3 9349 4106
Web: www.amsi.org.au